MICROCOPY RESOLUTION TEST CHART
NATIONAL BUREAU OF STANDARDS-1963-A

# Communications
# Research
# Centre

UNLIMITED
DISTRIBUTION
ILLIMITÉE

LEVEL

# A COMPARISON OF THE BURG AND THE KNOWN-AUTOCORRELATION AUTOREGRESSIVE SPECTRAL ANALYSIS OF COMPLEX SINUSOIDAL SIGNALS IN ADDITIVE WHITE NOISE

by

R.W. Herring

Sep 79

DDC
RECEIVED
JAN 31 1980
A

DEPARTMENT OF COMMUNICATIONS
MINISTÈRE DES COMMUNICATIONS

CRC REPORT NO. 1326

CANADA

OTTAWA, SEPTEMBER 1979

80

# COMMUNICATIONS RESEARCH CENTRE

DEPARTMENT OF COMMUNICATIONS
CANADA

# A COMPARISON OF THE BURG AND THE KNOWN-AUTOCORRELATION AUTOREGRESSIVE SPECTRAL ANALYSIS OF COMPLEX SINUSOIDAL SIGNALS IN ADDITIVE WHITE NOISE

by

R.W. Herring

(Radio and Radar Research Branch)

| Accession For | |
|---|---|
| NTIS G...I | |
| DDC TAB | |
| Unannounced | |
| Justification | |
| By | |
| Distribution/ | |
| Availability Codes | |
| Dist | Avail and/or special |
| A | |

## TABLE OF CONTENTS

# A COMPARISON OF THE BURG AND THE KNOWN-AUTOCORRELATION AUTOGRESSIVE SPECTRAL ANALYSIS OF COMPLEX SINUSOIDAL SIGNALS IN ADDITIVE WHITE NOISE

by

R.W. Herring

## ABSTRACT

Burg's algorithm for Maximum Entropy autoregressive spectral estimation is analyzed for the cases of one and two complex sinusoidal signals in additive white noise. For the latter case are found two biases which can account for the line splitting and line shifting that occur in simulation studies when the SNR is very high. These biases vanish completely if the two complex sinusoids are in phase quadrature at the middle of the data record; if there is an integral number of half-cycles of difference frequency contained in the data record, then the power level of the spectral estimate will be biased although the effects believed to cause splitting and shifting will be eliminated. Results of simulation studies to support these conjectures are presented.

## 1. INTRODUCTION

The Burg algorithm for the autoregressive spectral analysis of time-series data[1,2,3], sometimes referred to as the maximum-entropy method (MEM), is known to be inappropriate for the case of sinusoidal signals in additive white noise. This inappropriateness had been demonstrated both theoretically[4-6] and in practice[7-9]. A theoretically correct model[4-6] for the generating process for an N-pole complex sinusoidal signal in additive white noise is an N-pole, N-zero network with identical gain weights in its feedback (pole) and feed-forward (zero) parts, being excited with a white-noise input (see Figure 1). Autogressive analysis models the generating process for the data as an all-pole network excited by white noise. Since a zero in the generating process network can be simulated exactly only by an infinite number of poles, it is clear that when autoregressive analysis is used, in principle an infinite set of either autocorrelation or time series data must be used in order to achieve correct results.
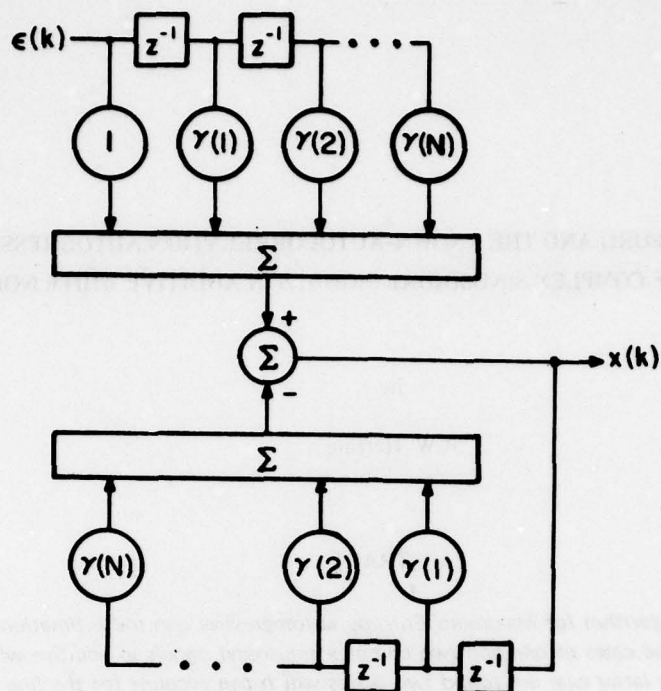
1

2



Figure 1. Network for generating N complex sine waves in additive white noise from complex white noise input
(after Figure 4.1 of Reference 6)

Fougere[9] has stated that, in the high signal-to-noise ratio (SNR) case, the Burg algorithm is overconstrained. In the case of simulation studies, this overconstraint causes errors in the estimated frequencies of spectral lines and the false splitting of spectral lines known to have been generated by a single pole (or a pair of poles, in the case of real signals). Fougere has developed an algorithm which avoids this phenomenon, but the algorithm is based on a gradient-search technique which lacks the intrinsic efficiency of the unmodified Burg algorithm.

In spite of its known limitations, the Burg algorithm is often used because of its computational efficiency. This report explores analytically the expected response of the Burg algorithm to time-series data comprising one or two complex sinusoids, with and without the presence of additive white noise. It is shown that only in very special cases does the Burg algorithm lead to the same results as are achieved when the true autocorrelation functions of the signals are known.

## 2. REVIEW OF AUTOREGRESSIVE SPECTRAL ANALYSIS

Autoregressive spectral analysis is based on the idea that, if it is somehow possible to design a feedforward (all-zero) filter which has as its input the data to be analyzed, and has as its output random white noise, then the power spectrum of the input data is given by the reciprocal of the power

transfer function of the filter.  Since this filter accounts for all the predictability inherent in the input signal and has as its output only unpredictable random white noise, it is often referred to as a prediction-error filter (PEF).

There are several well-known techniques for estimating the PEF corresponding to a given set of data.  When only amplitude time-series data are available, most of these depend upon estimates of the autocorrelation function derived from the time-series data.  The Burg algorithm, however, attempts to avoid possible biases or inconsistencies in such estimates of the autocorrelation function by deriving an estimate of the PEF coefficients directly from the data.

In this report the algorithm for generating the PEF when the true autocorrelation function is known is reviewed in Section 2.1 and the Burg algorithm is reviewed in Section 2.2.  The results from these sections are then used to generate the sets of PEFs corresponding to the cases of one and two complex sinusoids in additive white noise, and the properties of these sets of PEFs are compared and contrasted.

## 2.1  THE KNOWN-AUTOCORRELATION (KA) ALGORITHM[10,11]

Let it be assumed that N equispaced samples R(n) of the complex autocorrelation function have been given, for n=0,1,2,...,N-1, where N may be finite or infinite.  It is assumed that the Nyquist sampling criterion has been met.  Then the system of equations to be solved is

$$- \sum_{m=0}^{M} R(k-m)\alpha(m,M) = P(M)\delta(k) \qquad (1)$$

$$0 \leq k \leq M$$
$$0 \leq M \leq N-1$$

where the $\alpha(m,M)$s for m=0,1,2,...,M are sets of PEF coefficients, each value for M denoting a different set; the P(M)s are called the output error powers and are real; and $\delta(k) = 1$ if k=0, $\delta(k) = 0$ otherwise, is the Kroenecker delta function.  In order to maintain proper scaling, the leading terms of the PEFs, $\alpha(0,M)$, M=0,1,...,N-1, are set equal to -1 by definition.

Since negative indices for R(k-m) occur in the set of equations (1), it is necessary to note that $R(-n) = R*(n)$, where the asterisk (*) denotes complex conjugation.  This last fact allows (1) to be rewritten in the alternative form:

$$- \sum_{m=0}^{M} R(k'+m)\alpha*(m,M) = P(M)\delta(k') \qquad (2)$$

$$-M \leq k' \leq 0$$
$$0 \leq M \leq N-1$$

4

Equations (2) imply that the same result is obtained if the complex conjugate of a PEF is applied to the time-reversed autocorrelation data. This "reverse-conjugate" symmetry is used in the derivation of the Burg algorithm.

If the set of linear equations (1) for a particular value of M is written in matrix form, it can be seen that the matrix of autocorrelation samples $[R(k,m)]$, where $R(k,m) = R(k-m)$, is an MxM Toeplitz matrix. Therefore (1) can be solved by applying the algorithm developed by Levinson, Robinson and Durbin, otherwise known as the Levinson recursion. Following[11] the recursive solution to (1) can be written as:

$$P(0) = R(0) \tag{3a}$$

$$\alpha(M,M) = - \sum_{m=0}^{M-1} \alpha(m,M-1)R(M-m)/P(M-1) \tag{3b}$$

$$\alpha(m,M) = \alpha(m,M-1) - \alpha(M,M)\alpha^*(M-m,M-1) \tag{3c}$$

$$P(M) = (1 - |\alpha(M,M)|^2)P(M-1) \tag{3d}$$

$$m = 1,2,\ldots,M-1$$
$$M = 1,2,\ldots$$

Note that at each successive stage of the recursion, the introduction of one new autocorrelation sample, $R(M)$, generates but one independent value $\alpha(M,M)$ for the $M^{th}$-order PEF; all other coefficients of the $M^{th}$-order PEF are determined from linear combinations of the coefficients of the $(M-1)^{th}$-order PEF and their complex conjugates, using $\alpha(M,M)$ as indicated by (3c).

The $\alpha(M,M)$s are sometimes referred to as the reflection coefficients, because of the analogy of their appearance in (3d) with a similar equation which occurs in the theory of a signal propagating through a layered medium and being partially reflected at each layer interface.

In executing the recursion of equations (3a-d) it can occur (at least in theory) that, for some particular value of M, say $M_0$, $P(M_0) = 0$. This implies that $|\alpha(M_0,M_0)| = 1$. This condition can arise only in the case where the signal being analyzed can be modelled as $M_0$ complex sinusoids with no additive noise (see Sections 3.1 and 3.2); in general $M_0$ is not finite. In particular, $M_0$ cannot be finite when additive white noise is present[4].

For each order M of PEF, an estimate of the power spectrum based on (M+1) values of the autocorrelation function is given by

$$X_{KA}(\omega,M) = \frac{P(M)}{\left| \sum_{m=0}^{M} \alpha(m,M)\exp(-jm\omega) \right|^2} \tag{4}$$

where $\omega$ is the normalized angular frequency in radians with $-\pi < \omega \leq \pi$, and the subscript KA refers to the known-autocorrelation case. As discussed in Section 2.0 and as examination of (1) will indicate, the PEFs are "spiking" or whitening filters, since all but one of their output values are zero. The power spectrum of such an output signal is independent of frequency, or "white". The denominator in the right-hand term of (4) is the power transfer function of the PEF, which if multiplied by $X_{KA}(\omega,M)$, the estimated spectrum of the signal, yields the constant, white-noise spectrum $P(M)$. Thus, since both $P(M)$ and the power spectrum of the PEF can be calculated, the signal power spectrum $X_{KA}(\omega,M)$ can be estimated from (4) for successively higher orders of PEF.

## 2.2 THE BURG ALGORITHM

The Burg algorithm is a procedure for estimating the reflection coefficients directly from a set of time-series amplitude data. It avoids the biases introduced into the spectral estimate when the autocorrelation is estimated from the data and the known-autocorrelation algorithm is then applied; however, as is shown in Sections 4.1 and 4.2, the Burg algorithm introduces biases of its own sort.

Let it be assumed that a set of N time-series amplitude data $x(n)$, $n=0,1,2,\ldots,N-1$ have been given, and that $\langle x(n)\rangle = 0$, where the brackets $\langle \rangle$ denote expected value. The PEFs are derived sequentially. Each successively higher order PEF is applied to the data in both directions simultaneously, and the average of its forward and backward output error powers is minimized by adjusting only its reflection coefficient. The remaining coefficients of each PEF depend on the sequence of reflection coefficients through the functional relationship defined by (3c). The motivation for this procedure is its analogy with that defined by (1), (2), and (3a-d).

Following e.g.,[3,11-14] and taking proper note of the occurrences of complex conjugation in the complex data case, the Burg algorithm can be written in a lattice-filter formulation:

$$f_M(n) = f_{M-1}(n) - \beta(M,M)b_{M-1}(n-1) \qquad (5a)$$

$$b_M(n) = b_{M-1}(n-1) - \beta^*(M,M)f_{M-1}(n) \qquad (5b)$$

$$n = M,M+1,\ldots,N-1$$
$$M = 1,2,\ldots,N-1$$

and

$$f_o(n) = x(n) = b_o(n) \qquad (5c)$$

$$n = 0,1,2,\ldots,N-1$$

(See Figure 2, where $z^{-1}$ denotes the unit time-delay operator.) The series $f_M(n)$ is the output from the $M^{th}$-order PEF applied to the input signal $x(n)$

in the forward direction, and is expressed in terms of the output series from the $(M-1)^{th}$-stage of the lattice. The series $b_M(n)$ is the output from the $M^{th}$-order PEF, conjugated and applied to the input data in the reverse or backward direction, and again is expressed in terms of the output series from the $(M-1)^{th}$-stage of the lattice. The $\beta(M,M)$s are the reflection coefficients.
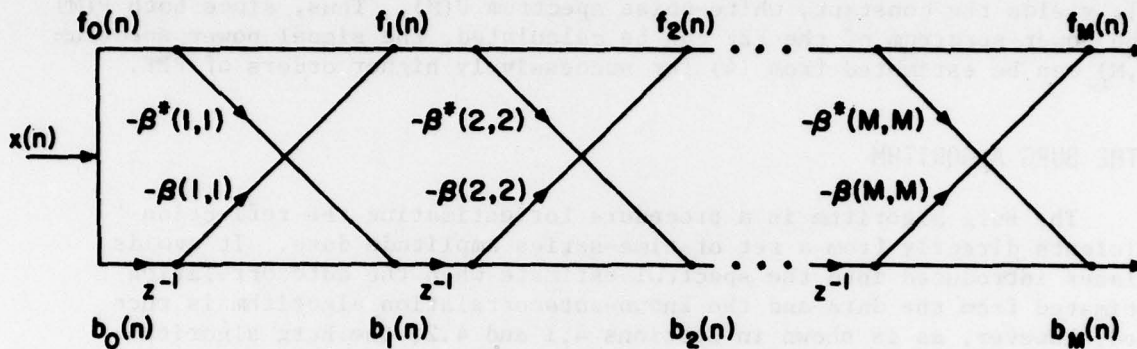


Figure 2. Basic all-zero lattice network
(after Reference 11)

The sum of the forward and backward output error energies at each stage of the lattice is given by

$$E(M) = \sum_{n=m}^{N-1} (|f_M(n)|^2 + |b_M(n)|^2)$$   (6)

$$M = 0,1,2,\ldots,N-1$$

The formula for computing $\beta(M,M)$, the Burg estimate of the $M^{th}$-order reflection coefficient, is derived by substituting eqns. (5a) and (5b) into (6), setting $[\partial E(M)/\partial \beta^*(M,M)] = 0$ and solving for $\beta(M,M)$.

$$\beta(M,M) = \frac{2 \sum_{n=M}^{N-1} b^*_{M-1}(n-1)f_{M-1}(n)}{\sum_{n=M}^{N-1} (|b_{M-1}(n-1)|^2 + |f_{M-1}(n)|^2)}$$   (7)

Notice the similarity of (7) to a single-lag unwindowed cross-correlation of the forward and backward output series.

In order to obtain spectral estimates, it is usual to let the output error powers π be defined as

$$\pi(0) = E(0)/(2N) \qquad (8a)$$

and

$$\pi(M) = (1 - |\beta(M,M)|^2)\pi(M-1) \qquad (8b)$$

$$M = 1,2,\ldots,N-1$$

by analogy with (3a) and (3d) respectively. Then, letting the β(M,M)s be defined by

$$\beta(m,M) = \beta(m,M-1) - \beta(M,M)\beta*(M-m,M-1) \qquad (9)$$

$$m = 1,2,\ldots,M-1$$

by analogy with (3c), and β(0,M) = -1 by definition, the M$^{th}$-order Burg power spectrum estimate X$_B$(ω,M) is given by

$$X_B(\omega,N) = \frac{\pi(M)}{\left[\sum_{m=0}^{M} \beta(m,M)\exp(-jm\omega)\right]^2} \qquad (10)$$

by analogy with (4).

## 2.3  THE ZEROES OF THE PREDICTION-ERROR FILTERS (PEFs)

By employing standard z-transform techniques, the z-transforms of the PEFs for the KA case and the Burg case can be written as polynomials in the complex variable z.  For the KA case, this polynomial is F$_{KA}$(z,M) where

$$F_{KA}(z,M) = 1 - \sum_{m=1}^{M} \alpha(m,M)z^{-m} \qquad (11)$$

Then (4) can be rewritten as

$$X_{KA}(\omega,M) = P(M)/|F_{KA}[\exp(j\omega),M]|^2 \qquad (12)$$

where the denominator is the squared magnitude of F$_{KA}$(z,M) evaluated around the unit circle (|z| = 1).  Similarly, for the Burg case, the polynomial is F$_B$(z,M), where

$$F_B(z,M) = 1 - \sum_{m=1}^{M} \beta(m,M)z^{-m} \qquad (13)$$

and (10) can be rewritten as

$$X_B(\omega,M) = \pi(M)/|F_B[\exp(j\omega),M]|^2 \qquad (14)$$

It is apparent from (12) and (14) that if any zeroes of $F_{KA}(z,M)$ or $F_B(z,M)$ lie near or on the unit circle, then the magnitude of the spectral estimators $X_{KA}(\omega,M)$ or $X_B(\omega,M)$ will be large at locations on the unit circle in the vicinity of such zeroes. Conversely, zeroes lying close to the origin of the complex z-plane will have little influence on the peaks of the spectrum, but will affect its magnitude away from the peaks. Thus some insight into the character of an autoregressive spectral estimate can be gained by studying the locations of the zeroes of its associated PEF.

## 3. THE ONE-POLE COMPLEX SINUSOID CASE

The formula for a complex signal $(x_1(n))$ consisting of a single complex sinusoid in the presence of additive white noise is given by

$$x_1(n) = A_1 \exp(jn\omega_1) + \varepsilon(n) \qquad (15)$$

where n is any positive or negative integer, or zero; $A_1$ is the complex amplitude of the complex sinusoid; $\omega_1$ is the angular frequency of the complex sinusoid, normalized so that $-\pi < \omega_1 \leq \pi$; and $\varepsilon(n)$ is additive white noise having the property

$$\langle \varepsilon^*(n)\varepsilon(n+k) \rangle = |\varepsilon|^2 \delta(k) \qquad (16)$$

where $|\varepsilon|^2$ is used to denote the variance of $\varepsilon(n)$ and $\delta(k)$ is again the Kroenecker delta function.

### 3.1 THE KA ESTIMATE OF THE PEF

The autocorrelation function $R_1(k)$ of the signal defined by (15) is given by

$$R_1(k) = |A_1|^2 \exp(jk\omega_1) + |\varepsilon|^2 \delta(k) \qquad (17)$$

where k is any positive or negative integer, or zero, and in general R(k) is defined by

$$R(k) = <x^*(n)x(n+k)> \qquad (18)$$

Substitution of (17) into (3a) gives the result

$$P_1(0) = |\epsilon|^2(\sigma_1^2 + 1) \qquad (19)$$

where $\sigma_1^2 = |A_1|^2/|\epsilon|^2$ is the signal-to-noise ratio (SNR). If there is no noise, i.e. $|\epsilon|^2 = 0$, then $P_1(0) = |A_1|^2$.

The following general result can be derived from (3b), (3c) and (3d) when $|\epsilon|^2 \neq 0$ and $|A_1|^2 \neq 0$:

$$\alpha_1(m,M) = [\sigma_1^2/(M\sigma_1^2+1)]\exp(jm\omega_1) \qquad (20a)$$

$$= [1/(M+\sigma_1^{-2})]\exp(jm\omega_1) \qquad (20b)$$

and

$$P_1(M) = |\epsilon|^2 \left\{ [(M+1)\sigma_1^2+1]/[M\sigma_1^2+1] \right\} \qquad (21)$$

$$M = 1,2,3,\ldots,\infty$$
$$m = 1,2,3,\ldots,M$$

In the noise-free case ($|\epsilon|^2 \to 0$ and $\sigma_1^2 \to \infty$), (20a) or (20b) imply that $\alpha_1(1,1) = \exp(j\omega_1)$ so that $|\alpha_1(1,1)|^2 = 1$. Then (3d) implies that $P_1(1) = 0$. Thus, for this special case, the sequences defined by (20) and (21) terminate at M=1. Otherwise for this signal model the sequences are infinite, with $P_1(M) \to |\epsilon|^2(1+M^{-1})$ as $M\sigma_1^2 \to \infty$.

The z-transform of the KA PEF (cf. (11))

$$F_{KA}^{(1)}(z,M) = 1 - [\sigma_1^2/(M\sigma_1^2+1)] \sum_{m=1}^{M} z^{-m}\exp(jm\omega_1) \qquad (22)$$

where the superscript 1 denotes a one-pole complex sinusoidal signal. For M=1, $F_{KA}^{(1)}(z,1)$ has a zero at $z_0=[\sigma_1^2/(\sigma^2+1)]\exp(j\omega_1)$. For M=2, $F_{KA}^{(1)}(z,2)$ has zeroes at.

$$z_0 = \left\{ \frac{-2\sigma_1^2}{\sigma_1^2 \pm \sigma_1 \sqrt{9\sigma_1^2 + 4}} \right\} \exp(j\omega_1) \qquad (23)$$

so that for high SNR $(1 << \sigma_1^2 < \infty)$, the zeroes occur at approximately 1.0 $\exp(j\omega_1)$ and $-0.5 \exp(j\omega_1)$, and for low SNR $(\sigma_1^2 << 1)$, the zeroes occur at approximately $\pm\sigma_1 \exp(j\omega_1)$.

Some algebraic manipulation shows that, for the product $M\sigma_1^2$ sufficiently greater than 1, an approximate root $z_0$ of (22) is given by

$$z_0 \simeq \left[1 - \frac{2}{(M-1) \, M\sigma_1^2}\right] \exp \, (j\omega_1) \qquad (24)$$

This means that, as $M\sigma_1^2 \to \infty$, the estimated location of the pole corresponding to the single complex sinusoid asymptotically approaches the correct location $\exp(j\omega_1)$ on the complex z-plane along a radius oriented at an angle corresponding to the true frequency of the signal. This is true even when $\sigma_1^2 << 1$.

Numerical solutions of (24) show that the other zeroes tend to distribute themselves with approximately uniform angular separation and approximately constant radius inside the unit circle so as to account for the uniform spectrum of the additive white noise. The radius at which the zeroes occur varies inversely with the SNR.

## 3.2 THE BURG ESTIMATE OF THE PEF

Let it be assumed that N samples of the signal defined by (15) have been given:

$$x_1(n) = A_1 \, \exp(jn\omega_1) + \varepsilon(n) \qquad (25)$$

$$n = 0,1,2,\ldots,N-1$$

Substituting (25) into (6) by using (5c) and then taking the expected value of $E_1(0)$ yields

$$<E_1(0)> \, = \, 2N|\varepsilon|^2(\sigma_1^2+1) \qquad (26)$$

It is not so easy to calculate $<\beta_1(1,1)>$, since examination of (7) shows that it is necessary to derive the expected value of a quotient of correlated random variables. In general, this requires that the statistics of the random variables be specified and the problem be solved numerically. This will not be done here.

However, for sufficiently high SNR (e.g., $\sigma_1^2 > 100$ or 20 dB) the approximation $(1+x)^{-1} \sim 1-x$, where $x \sim \varepsilon(n)/A_1$, can be used to approximate the denominator of (7). Then the following approximate result, which is independent of the statistical distribution of the white noise $\varepsilon(n)$, is obtained:

$$\langle\beta_1(1,1)\rangle = \left\{1/[1+B_1(1,N)\sigma_1^{-2}]\right\}\exp(j\omega_1) \tag{27}$$

**where**

$$B_1(1,N) = (N^2-2)/(N-1)^2 \tag{28}$$

and $2 \geq B_1(1,N) > 1$ for $2 \leq N < \infty$. Comparison of (27) with (20b) for $M=1$ shows that for high SNR $\beta_1(1,1)$ is a biased estimate of $\alpha_1(1,1)$. However, $\beta_1(1,1)$ correctly estimates the angular frequency $\omega_1$ of the single complex sinusoid, and the bias term $B_1(1,N)$ monotonically approaches unity as $N$ becomes large.

From (26), (27) and (8a) and (8b) it can be shown that

$$\langle\pi_1(0)\rangle = |\varepsilon|^2(\sigma_1^2+1) \tag{29}$$

and, to the same degree of approximation as was used to obtain (27)

$$\langle\pi_1(1)\rangle = 2B_1(1,N)|\varepsilon|^2 \tag{30}$$

Comparison of (30) with (21) shows that $\pi_1(1)$ is a biased estimator of $P_1(1)$, since for $\sigma_1^2$ large, $P_1(1) \approx 2|\varepsilon|^2$.

The result (30) implies that the lattice-filter outputs $f_1(n)$ and $b_1(n)$ as defined by (5a) and (5b) have low SNR, since their expected power is at most only a factor of four greater than the additive white noise power $|\varepsilon|^2$. Therefore it would again be necessary to specify the detailed statistics of the additive noise before the higher order reflection coefficients could be estimated. This will not be done here.

## 3.3 DISCUSSION OF THE ONE-POLE COMPLEX SINUSOID CASE

The results of Sections 3.1 and 3.2 show that, for high SNR ($\sigma_1^2 > 100$) the first order ($M=1$) PEF generated by the Burg algorithm is biased as compared to the PEF generated by the KA technique. This bias, however, monotonically decreases as the number of data $N$ is increased, and both the KA and the Burg algorithms correctly estimate the frequency of the complex sinusoid.

It is impossible to investigate the properties of the Burg PEFs for the low SNR case, or for orders higher than $M=1$ for the high SNR case, without specifying the statistical distribution of the additive white noise. This problem has not been considered here.

## 4. THE TWO-POLE COMPLEX SINUSOID CASE

The sampled signal $x_2(n)$ consisting of two complex sinusoids in the presence of additive white noise is given by

$$x_2(n) = A_1 \exp(jn\omega_1) + A_2 \exp(jn\omega_2) + \epsilon(n) \qquad (31)$$

where $A_k = |A_k| \exp(j\phi_k)$ is the complex amplitude of the $k^{th}$ sinusoid, $\phi_k$ is its arbitrary initial phase at $n=0$, and $\omega_k$ is its angular frequency, normalized so that $-\pi < \omega_k \leq \pi$, for $k=1,2$. $\epsilon(n)$ is additive white noise, as in (15). It is apparent that if $A_2 = A_1^*$ and $\omega_2 = -\omega_1$ then $x_2(n)$ is a sampled real sinusoid in additive white (complex) noise.

Equation (31) can be written in a form which will be subsequently more tractable:

$$x_2(n) = A_o \exp[j(n\omega_o + \phi_o)]$$

$$\chi \left\{ r \exp[j(n\Delta\omega + \Delta\phi)] + r^{-1} \exp[-j(n\Delta\omega + \Delta\phi)] \right\} + \epsilon(n) \qquad (32)$$

where $A_o = |A_1 A_2|^{\frac{1}{2}}$ is the geometric mean of the magnitudes of the two amplitudes; $r = [|A_1|/|A_2|]^{\frac{1}{2}}$ is the square root of the ratio of the magnitudes of the amplitudes; $\phi_o = (\phi_1 + \phi_2)/2$ is the arithmetic mean of the initial phases; $\Delta\phi = (\phi_1 - \phi_2)/2$ is one-half the difference between the two phases; $\omega_o = (\omega_1 + \omega_2)/2$ is the arithmetic mean of the two angular frequencies; and $\Delta\omega = (\omega_1 - \omega_2)/2$ is one-half the difference between the two frequencies.

## 4.1 THE KA ESTIMATE OF THE PEF

The autocorrelation function $R_2(k)$ of the signal defined by (32) is given by

$$R_2(k) = A_o^2(r^2 + r^{-2}) \exp(jk\omega_o)[\cos k\Delta\omega + j\rho(r)\sin k\Delta\omega] + |\epsilon|^2 \delta(k) \qquad (33)$$

where

$$\rho(r) = (r^2 - r^{-2})/(r^2 + r^{-2}) \qquad (34)$$

and $k$ is any positive or negative integer, or zero. Substitution of (33) into (3a) gives the result

$$P_2(0) = |\epsilon|^2(\sigma_2^2 + 1) \qquad (35)$$

where $\sigma_2^2 = A_o^2(r^2 + r^{-2})/|\epsilon|^2$ is the SNR. If there is no noise, then $P_2(0) = A_o^2(r^2 + r^{-2})$ is the signal power.

From (33), (35), (3b) and (3d), the following general results for the reflection coefficient and the output error power for M=1 can be derived when $|\epsilon|^2 \neq 0$ and $A_o \neq 0$:

$$\alpha_2(1,1) = \exp(j\omega_o)\left\{[\cos\Delta\omega + j\rho(r)\sin\Delta\omega]/[1 + \sigma_2^{-2}]\right\} \tag{36}$$

and

$$P_2(1) = A_o^2(r^2+r^{-2})\left\{[1-\rho^2(r)]\sin^2\Delta\omega + \sigma_2^{-2}(2+\sigma_2^{-2})\right\}/\left\{1+\sigma_2^{-2}\right\} \tag{37}$$

For high SNR ($\sigma_2^2 \gg 1$), the first reflection coefficient is given approximately by

$$\alpha_2(1,1) = \exp(j\omega_o)[\cos\Delta\omega + j\rho(r)\sin\Delta\omega] \tag{38}$$

For $r=1$, $\rho(r) = 0$ and the zero of $F_{RA}^{(2)}(z,1)$ (see Section 2.3) is located at $z_o = \cos\Delta\omega \, \exp(j\omega_o)$, which lies on a radius oriented at the mean angular frequency $\omega_o$. This zero moves towards the limiting values of $\exp(j\omega_1)$ as $r\to\infty$ and $\rho(r) \to 1$, or $\exp(j\omega_2)$ as $r\to 0$ and $\rho(r) \to -1$, and the single complex sinusoid case is approached in each case.

The output error power is, using (38), (35) and (8b),

$$P_2(1) = (2A_o \sin\Delta\omega)^2/(r^2+r^{-2}) \tag{39}$$

which is essentially the signal power attenuated by the factor $[2\sin\Delta\omega/(r^2+r^{-2})]^2$. This factor is unity when $r=1$ and $\Delta\omega=\pm\pi/2$, and decreases as $r$ or $\Delta\omega$ deviate from these values.

For low SNR ($\sigma_2^2 \ll 1$), the reflection coefficient and the output error power are given by

$$\alpha_2(1,1) = \exp(j\omega_o)\sigma_2^2 \, [\cos\Delta\omega + j\rho(r)\sin\Delta\omega] \tag{40}$$

and

$$P_2(1) = |\varepsilon|^2 + A_o^2(r^2+r^{-2}) \tag{41}$$

Thus the frequency estimated from the location of the zero of the M=1 order PEF lies in the range bounded by $\omega_o \pm \Delta\omega$, and the output error power is essentially the unattenuated signal plus noise power.

For M=2, (33), (36), and (3b) can be combined to yield

$$\alpha_2(2,2) = -\exp(j2\omega_o)\left\{\frac{[1-\rho^2(r)]\sin^2\Delta\omega - \sigma_2^{-2}\,[\cos2\Delta\omega + j\rho(r)\sin2\Delta\omega]}{[1-\rho^2(r)]\sin^2\Delta\omega + \sigma_2^{-2}[2+\sigma_2^{-2}]}\right\} \tag{42}$$

and (37), (42) and (3d) can be combined to yield

14

$$P_2(2) = |\epsilon|^2 \frac{2[1-\rho^2(r)]\sin^2\Delta\omega(2 + \cos2\Delta\omega) + \sigma_2^{-2}(3+\sigma_2^{-2})}{[1-\rho^2(r)]\sin^2\Delta\omega + \sigma_2^{-2}(2+\sigma_2^{-2})} \qquad (43)$$

For high SNR ($\sigma_2^2 \gg 1$) and

$$\sigma_2^2[1-\rho^2(r)]\sin^2\Delta\omega \gg |\cos2\Delta\omega + j\rho(r)\sin2\Delta\omega| \qquad (44)$$

(42) reduces to

$$\alpha_2(2,2) = -\exp(j2\omega_0) \qquad (45)$$

It can be shown from (45), (36) and (3c) that

$$\alpha_2(1,2) = \exp(j\omega_0) \, 2\cos\Delta\omega \qquad (46)$$

so that, in the limit as the left-hand side of (44) approaches infinity, the zeroes of $F_{KA}^{(2)}$ approach $z_0 = \exp[j(\omega_0 \pm \Delta\omega)]$, the true locations of the poles of the complex sinusoids. In this same limit, $|\alpha_2(2,2)|^2 = 1$, so that $P_2(2)=0$ and the recursion terminates.

For the intermediate case, where $\sigma_2^2 \gg 1$ but (44) is not satisfied, i.e.,

$$\sigma_2^2[1-\rho^2(r)]\sin\Delta\omega \ll |\cos2\Delta\omega + j\rho(r)\sin2\Delta\omega| \qquad (47)$$

(42) can be reduced to

$$\alpha_2(2,2) = \exp(j2\omega_0)\cos\Delta\omega[0.5 \, \cos\Delta\omega + j\rho(r)\sin\Delta\omega] \qquad (48)$$

and it can be shown from (48), (38) and (3c) that

$$\alpha_2(1,2) = 0.5 \, \exp(j\omega_0)[\cos\Delta\omega + j\rho(r)\sin\Delta\omega] \qquad (49)$$

so that the zeroes of $F_{KA}^{(2)}(z,2)$ occur at $[\cos\Delta\omega + j\rho(r)\sin\Delta\omega]\exp(j\omega_0)$ and $-0.5[\cos\Delta\omega + j\rho(r)\sin\Delta\omega]\exp(j\omega_0)$. Comparison of these results with (23), which gives the zero locations of the PEF for a one-pole signal and M=1, shows that the intermediate case result for the two-pole signal is very similar to that for the one-pole signal at high SNR. Comparison with (38) shows that one of the zeroes of $F_{KA}^{(2)}(z,2)$ remains the same as that of $F_{KA}^{(2)}(z,1)$ at high SNR; i.e., the two poles are estimated as one by the M=2 PEF if (44) is not satisfied.

For the low SNR case ($\sigma_2^2 \ll 1$), (42) reduces to

$$\alpha_2(2,2) = \exp(j2\omega_o)\left\{\sigma_2^2[\cos2\Delta\omega + j\rho(r)\sin2\Delta\omega]\right\} \tag{50}$$

and $P_2(2)$ is the same as $P_2(1)$ as given by (41). Since for this case both $|\alpha_2(2,2)|$ and $|\alpha_2(1,1)|$ are proportional to $\sigma_2^2$, then from (3c) it is clear that, to first order in $\sigma_2^2$,

$$\alpha_2(1,2) = \alpha_2(1,1) \tag{51}$$

where $\alpha_2(1,1)$ is given by (40). The zeroes of $F_{KA}^{(2)}(z,2)$ in this case occur at approximately $z = \sigma_2\left\{\pm[\cos2\Delta\omega + j\rho(r)\sin2\Delta\omega]^{\frac{1}{2}} + \sigma_2[\cos\Delta\omega + j\rho(r)\sin\Delta\omega]/2\right\}$ $\exp(j\omega_o)$. For r=1 and thus $\rho(r)=0$, the zeroes occur at $z = \sigma_2\left\{\pm[\cos2\Delta\omega]^{\frac{1}{2}} + \sigma_2[\cos\Delta\omega]/2\right\}\exp(j\omega_o)$, which lie close to the origin of the complex z-plane, on a diameter of the unit circle passing through the point $z = \exp(j\omega_o)$. For $r \gg 1$ ($\rho(r) \rightarrow 1$) or $r \ll 1$ ($\rho(r) \rightarrow -1$) the zeroes tend to the locations $z = \sigma_2[\pm1 + \sigma_2/2]\exp(j\omega_1)$ or $z = \sigma_2[\pm1 + \sigma_2/2]\exp(j\omega_2)$ respectively. Thus it is apparent that for low SNR, the spectral estimate corresponding to M=2 is incapable of resolving the spectral peaks corresponding to the poles of the two complex sinusoidal signals.

There appears to be no straightforward recursion formula for the KA PEF coefficients, as in the case of the single sinusoid example of Section 3.1. Therefore, following this approach, it is not easy to determine the behavior of the KA PEFs in the case of large M and, in particular, whether resolution of the two sinusoids is to be expected for the product $M\sigma_2^2$ sufficiently large, independent of the value of $\sigma_2^2$. This problem, however, has been solved using powerful matrix techniques, by Marple[6].

## 4.2 THE BURG ESTIMATE OF THE PEF

Let it again be assumed (cf. Section 3.2) that N samples of the signal defined by (32) have been given:

$$x_2(n) = A_o \exp[j(n\omega_o + \phi_o)]\left\{r \exp[jn\Delta\omega+\Delta\phi)] + r^{-1}\exp[-j(n\Delta\omega+\Delta\phi)]\right\} + \varepsilon(n) \tag{52}$$

$$n = 0,1,2,\ldots,N-1$$

Substituting (52) into (6) and (7), using (5c), and then applying (8a) and taking expected values with respect to the additive white noise only yields

$$\langle\Pi_2(0)\rangle = A_o^2(r^2+r^{-2})[1 + 2\cos\Delta\phi_{mid}\, G(N,\Delta\omega)/(r^2+r^{-2})] + |\varepsilon|^2 \tag{53}$$

for the expected signal-plus-noise power. Here

$$G(N,\Delta\omega) = \frac{\sin(N\Delta\omega)}{N\sin\Delta\omega} \tag{54}$$

is the common grating-function frequency response of a normalized, uniformly weighted discrete Fourier transform of N data, and

$$\Delta\phi_{mid} = (N-1)\Delta\omega + 2\Delta\phi \qquad (55)$$

is the phase difference between the two complex sinusoidal components, reckoned at the middle of the data set. Note that there may or may not be a datum at the middle of the data set, according to whether N is an odd or even integer, respectively. Also note that $\Delta\phi$ has not been averaged, but rather is assumed to be a fixed parameter of the particular set of data being analyzed. This assumption corresponds to the usual practical case, where only one set of data is available.

Again, it is not easy to calculate the expected values of the reflection coefficients unless the assumption of high SNR is made. In that case the same approximations can be made as in the derivation of (26) to get

$$<\beta_2(1,1)> = \exp(j\omega_o) \left\{ \frac{\cos\Delta\omega + j\rho(r)\sin\Delta\omega + 2\,\cos\Delta\phi_{mid}\,G(N-1,\Delta\omega)/(r^2+r^{-2})}{1 + 2\,\cos\Delta\phi_{mid}\cos\Delta\omega\,G(N-1,\Delta\omega)/(r^2+r^{-2}) + \sigma_2^{-2}[1 + B_2(1,N)]} \right\}$$

$$(56)$$

where the bias term $B_2(1,N)$ is of order $(N-1)^{-1}$ and is given by eqn. (A1) of Appendix A.

Comparison of (56) and (36) shows that for high SNR $\beta_2(1,1)$ is a biased estimate of $\alpha_2(1,1)$ unless N→∞. For infinite SNR and finite N, however, $\beta_2(1,1)$ becomes an unbiased estimate of $\alpha_2(1,1)$ if

$$\cos\Delta\phi_{mid} = 0 \qquad (57)$$

or

$$G(N-1,\Delta\omega) = 0 \qquad (58)$$

Similarly, comparison of (53) and (35) shows that $\Pi_2(0)$ is a biased estimate of $P_2(0)$ unless either (57) is satisfied or

$$G(N,\Delta\omega) = 0 \qquad (59)$$

It is impossible to satisfy (58) and (59) simultaneously for N finite, but when (57) is satisfied the Burg spectral estimate (14) is unbiased for M=1 and infinite SNR.

Progressing now to the second stage (M=2) of the Burg algorithm, it is found that the algebra becomes all but intractable unless the condition of infinite SNR is assumed. For this special case, (56), (52), (5a-c) and (7) can be used to derive the following expression for $\beta_2(2,2)$:

$$\beta_2(2,2) = -\exp(j2\omega_o) \; \chi \; \left\{ \left\{ 1 - 2 \cos\Delta\phi_{mid} \, G(N-2,\Delta\omega)/(r^2+r^{-2}) \right\} \right.$$

$$-2 \cos\Delta\phi_{mid} G(N-1,\Delta\omega) \; \chi \; \left\{ \cos\Delta\phi_{mid} G(N-2,\Delta\omega)[\cos\Delta\omega + j\rho(r)\sin\Delta\omega] \right.$$
$$\left. - 2 \cos\Delta\omega/(r^2+r^{-2}) \right\}$$

$$+ \cos^2\Delta\phi_{mid} G^2(N-1,\Delta\omega) \; \chi \; \left\{ [\cos2\Delta\omega + j\rho(r)\sin2\Delta\omega] \right.$$
$$\left. \left. -2\cos\Delta\phi_{mid} G(N-2,\Delta\omega)/(r^2+r^{-2}) \right\} \right\}$$

$$\Bigg/ \left\{ \left\{ 1 - 2\cos\Delta\phi_{mid} G(N-2,\Delta\omega)/(r^2+r^{-2}) \right\} \right.$$

$$-2\cos\Delta\phi_{mid} \cos\Delta\omega G(N-1,\Delta\omega) \; \chi \; \left\{ \cos\Delta\phi_{mid} G(N-2,\Delta\omega) - 2/(r^2+r^{-2}) \right\}$$

$$\left. + \cos^2\Delta\phi_{mid} G^2(N-1,\Delta\omega) \; \chi \; \left\{ 1 - 2\cos\Delta\phi_{mid} \cos2\Delta\omega G(N-2,\Delta\omega)/(r^2+r^{-2}) \right\} \right\}$$

$$(60)$$

Examination of (60) shows that, even for infinite SNR, the "correct" value of $-\exp(j2\omega_0)$ for the reflection coefficient $\langle\beta_2(2,2)\rangle$ is not realized for N finite unless either (57) or (58) is satisfied. Realization of either of these conditions for infinite SNR will, as examination of (60) shows, cause the magnitude of the reflection coefficient to be unity. Thus it can be inferred that, for sufficiently high SNR, the two crucial factors affecting the reflection coefficient computed using the Burg algorithm are the phase difference between the two complex sinusoids at the middle of the data record, $\Delta\phi_{mid}$, and the number of cycles of difference frequency contained in the finite length data record.

## 4.3  DISCUSSION OF THE TWO-POLE COMPLEX SINUSOID CASE

The results of Section 4.1 and 4.2 show that even for infinite SNR, the first (M=1) and the second (M=2) order PEFs generated by the Burg algorithm are biased as compared to the PEFs generated by the KA technique. It is clear from the appearance of the grating function (54) in the equations (56) and (60) for the first and second-order reflection coefficients that the magnitude of such biases will have inverse dependence on N, the length of the data record.

The effect of this bias is to reduce the magnitude of the reflection coefficient and thus to allow significant levels of uncancelled signal energy to propagate beyond the stage M=2 in the Burg algorithm. Then PEFs of successively higher order can be based on this coherent "leakage" signal. However, whenever one of the criteria described by (57) or (58) is satisfied, no significant coherent leakage signal is propagated beyond the stage M=2. It is conjectured that it is the presence or absence of this coherent leakage signal beyond the stage M=2 that determine whether or not line splitting will occur for PEFs of some higher order. Results both of previously published[7,8] and new simulation studies support this conjecture, as indicated in Section 5.

## 5. RESULTS OF SOME SIMULATION STUDIES

In this Section are presented the results of some studies of the performance of the complex Burg algorithm for the analysis of signals known to be comprised of two complex sinusoids in the presence of very weak additive complex white noise ($\sigma_2^2$ = 77 dB). These studies parallel and extend a set of studies performed by Fougere et al.[8] using the real-arithmetic Burg algorithm to estimate spectra of a single real sine-wave signal in the presence of very weak additive real white noise.

It will be necessary to make comparisons between complex data of the form (52) and real data $x_s(n)$ of the form

$$x_s(n) = \sin(n\omega_s + \phi_s) + \epsilon_s(n) \tag{61}$$

$$n = 0,1,\ldots,N-1$$

which is comprised of N samples of a real sine wave with initial phase $\phi_s$ plus additive uncorrelated noise samples $\epsilon_s(n)$. The angular frequency $\omega_s$ is given by

$$\omega_s = 2\pi f\Delta t \tag{62}$$

where $\Delta t$ is the sampling interval (sec) and f is the signal frequency (Hz). Equation (61) can easily be rewritten in the form of (52) by letting $A_o$ = 0.5, r=1, $\phi_0$ = 0, $\Delta\phi = \phi_s - \pi/2$, $\omega_0$ = 0 and $\Delta\omega = \omega_s$. Then the phase difference between the two complex components of the sine wave reckoned at the middle of the data record is, according to (55), given by

$$\Delta\phi_{mid} = (N-1)\omega_s + 2\phi_s -\pi \tag{63}$$

The results of Fougere et al. have been extended by allowing the value of $r^2$, the ratio of the positive frequency to negative frequency signal amplitude, to range from 1 to $\infty$ in a series of six steps. These steps are denoted by the letters A-F, and the relevant signal parameters are summarized in Table 1. For all steps the total signal power $A_o^2(r^2+r^{-2})$ was maintained constant and equal to 0.5, the power of a real unit-amplitude sine wave. Also, the values of $\phi_0$ = 0 and $\omega_0$ = 0 were maintained for all the trials. These restrictions do not limit the generality of the results obtained. It is clear that an arbitrary phase rotation of the entire data-set will have no effect on its power spectrum. It is also clear that since terms of the form $\exp(jm\omega_0)$ can be factored out of the $\alpha(m,M)$s and $\beta(m,M)$s, the effect of non-zero $\omega_0$ is simply to shift the estimated spectrum along the frequency axis (in a circular or end-around fashion) by the amount $\omega_0$. Finally, it should be noted that for each set of cases examined, the same set of noise-data samples was used with all sets of signal data.

### TABLE 1
#### Test-case Signal Parameters

| CASE | r | $\rho(r)$ | $r^2+r^{-2}$ |
|------|------|--------|-----------|
| A | 1 | 0 | 2 |
| B | $\sqrt{2}$ | 0.6 | 2.5 |
| C | $\sqrt{10}$ | 0.98 | 10.1 |
| D | $\sqrt{100}$ | 0.9998 | 100.01 |
| E | $\sqrt{1000}$ | 0.999998 | 1000.001 |
| F | $\infty$ | 1 | $\infty$ |

## 5.1 CASE 1

The signal data for Case 1 consisted of 21 samples of two complex sinusoids with angular frequencies $\omega_{1,2} = \pm 2\pi/20$, so that $\Delta\omega = \omega_1$. $\Delta\phi_{mid}$ was stepped from $-\pi$ to $+\pi$ in increments of $2\pi/9$ radians, so that in all instances $\cos\Delta\phi_{mid} \neq 0$. All spectra were estimated using (14) and a length 20 (M=19) Burg PEF.

For Case 1A (r=1) the situation corresponds closely to that of Fougere et al.'s Case 2, where 21 samples of a 1 Hz real sine wave sampled at intervals of $\Delta t = 0.05$ s were analyzed, and $\phi_s$ was stepped from 0 to $\pi$ radians in steps of $\pi/9$ radian (20°). However, they used uncorrelated real noise samples uniformly distributed over the range $[-10^{-4}, 10^{-4}]$, thus having a slightly higher SNR (82 dB) than that used here (77 dB). Also, they analyzed their data using a real-arithmetic implementation of the Burg algorithm.

The effects of the relaxation of the conjugate symmetry forced on the spectrum by the use of real data and real arithmetic analysis are apparent as asymmetries in Figure 3, which shows a perspective projection of the set of 10 spectra viewed as though looking between two parallel rows of pillars. $\Delta\phi_{mid}$ is increasing "into" the page, and $\omega$ is increasing from left to right as indicated. The vertical scale is, of course, distorted by the perspective projection; the long and short vertical bars indicate 20 dB variation in power spectral density in the first and tenth spectra respectively.

Figures 4 to 8 show similarly displayed spectra for Cases 1B-F, where r is increasing as shown in Table 1. In all cases the signal frequencies were accurately estimated by unsplit spikes, although there was some variability of the magnitude of the spikes, particularly for the larger values of r. However, examination of the locations of the zeroes of the PEFs showed that in all cases the zeroes of the PEF varied by no more than $2\times10^{-3}$ radians from the known locations of the signal poles.

The suggestion of Johnson and Andersen[15] of computing and examining the residues of the poles of the spectral estimator (14) showed that the
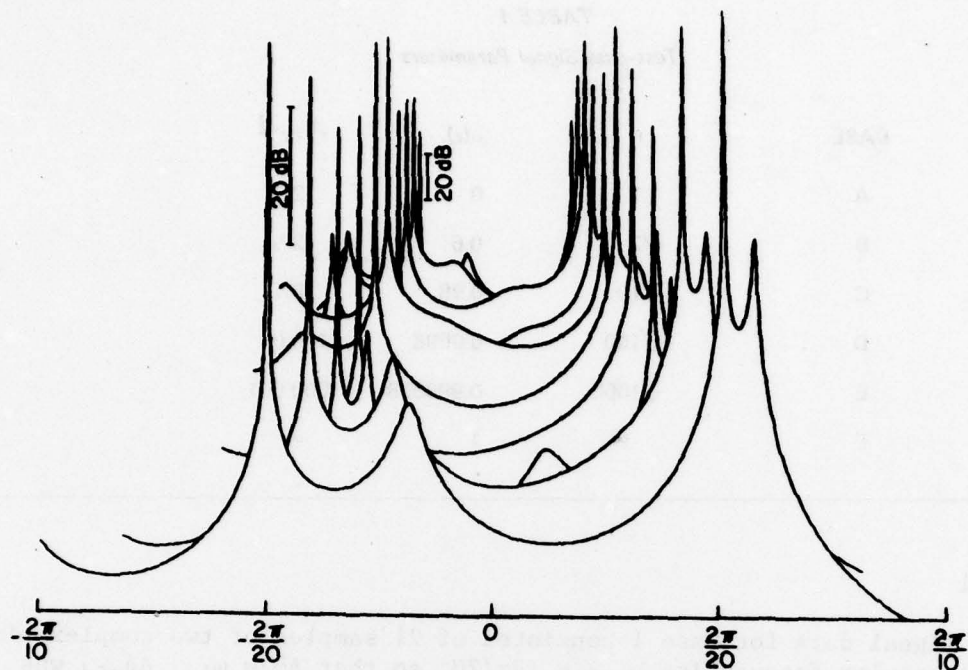
Figure 3. Case 1A. Estimated spectral power vs. angular frequency and $\Delta\phi_{mid}$. $\omega_1 = -\omega_2 = 2\pi/20$. N = 21. M = 19. $\Delta\phi_{mid}$ stepped from $-\pi$ to $\pi$ in increments of $2\pi/9$ radians. r = 1. (Perspective projection.)
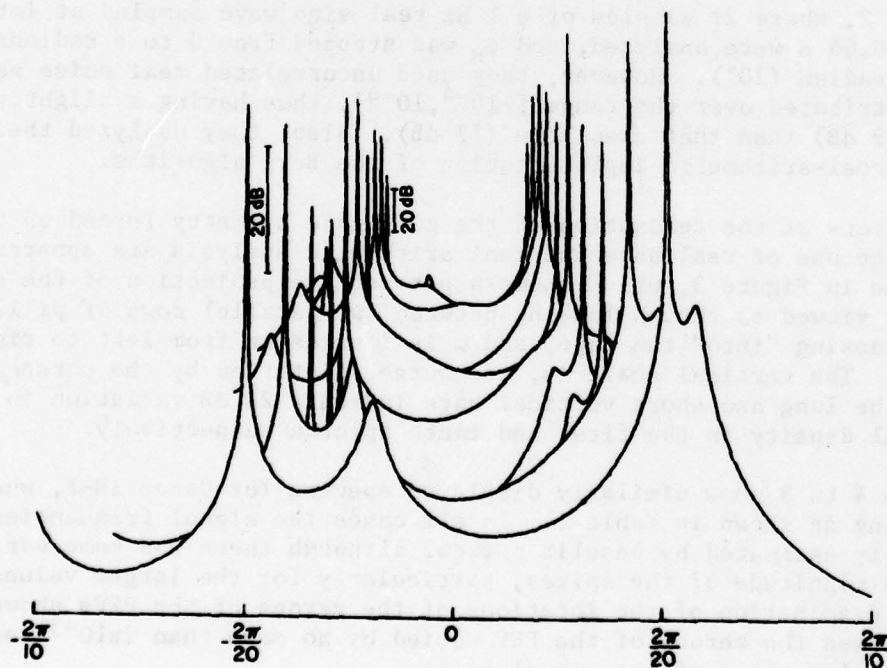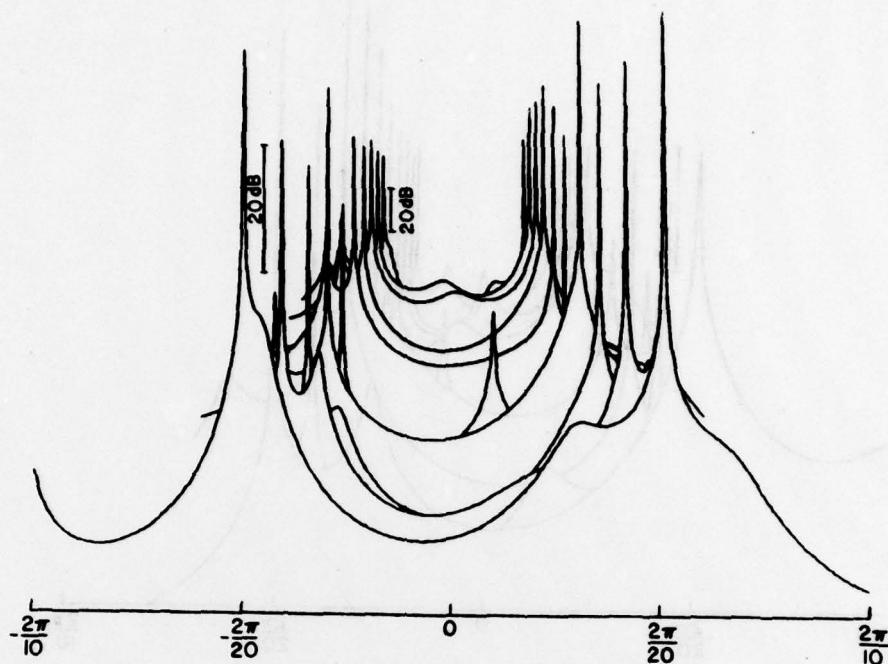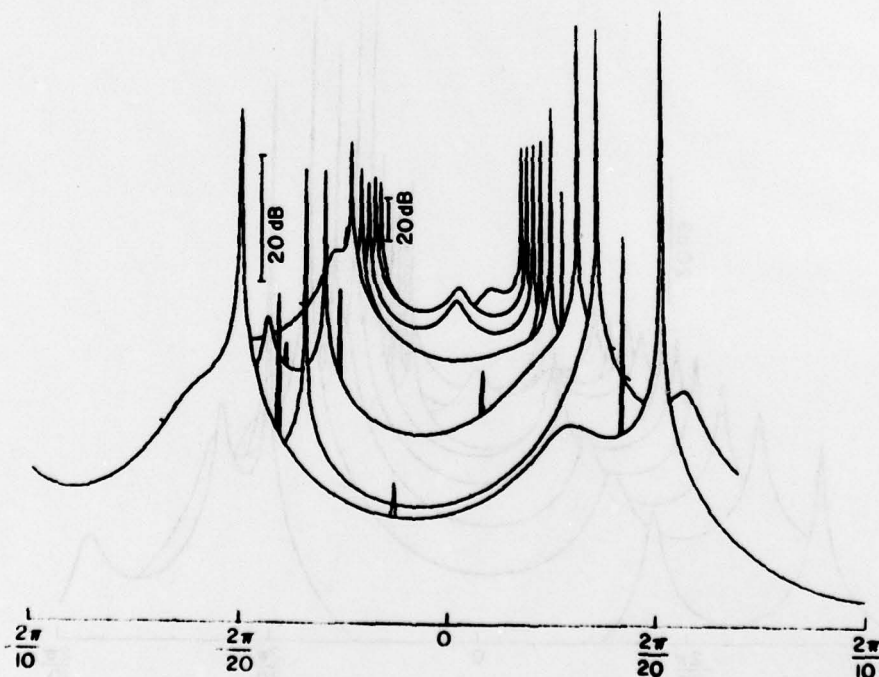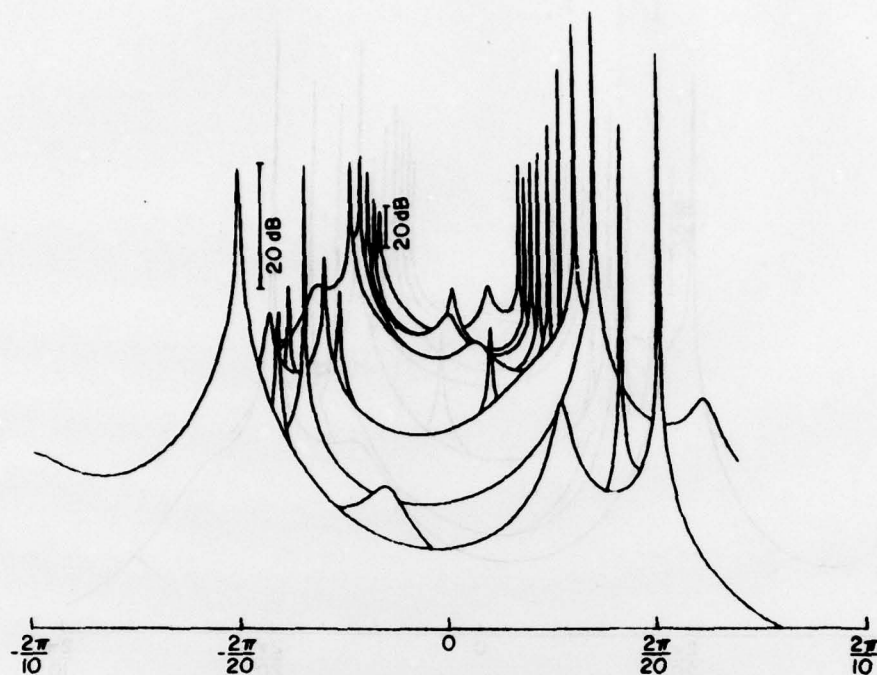


Figure 4. Case 1B. Estimated spectral power vs. angular frequency and $\Delta\phi_{mid}$. $\omega_1 = -\omega_2 = 2\pi/20$. N = 21. M = 19. $\Delta\phi_{mid}$ stepped from $-\pi$ to $\pi$ in increments of $2\pi/9$ radians. r = $\sqrt{2}$. (Perspective projection.)

Figure 5. Case 1C. Estimated spectral power vs. angular frequency and $\Delta\phi_{mid}$. $\omega_1 = -\omega_2 = 2\pi/20$. N = 21. M = 19. $\Delta\phi_{mid}$ stepped from $-\pi$ to $\pi$ in increments of $2\pi/9$ radians. $r = \sqrt{10}$. (Perspective projection.)
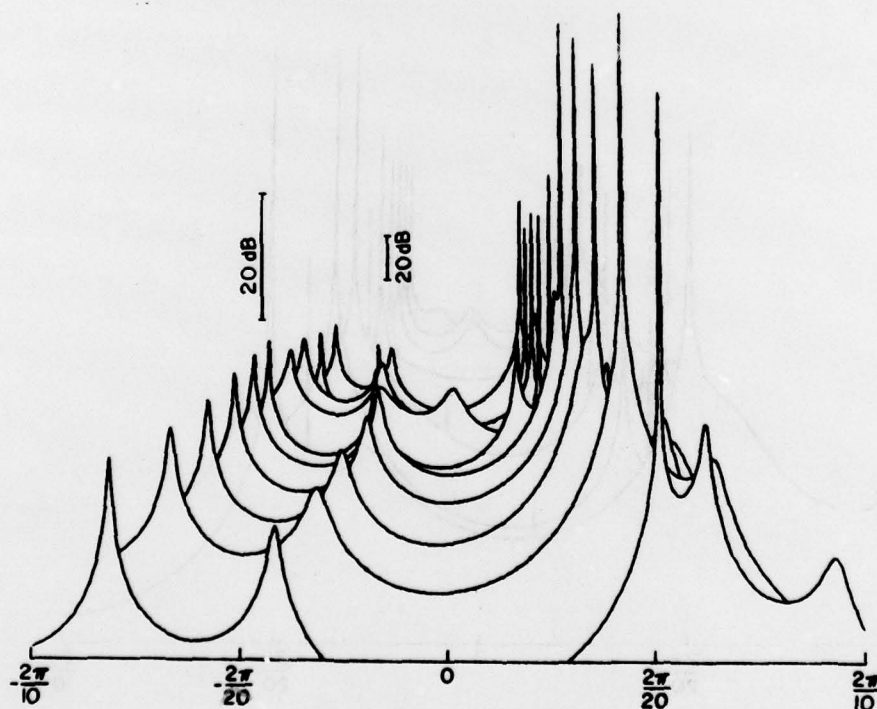


Figure 6. Case 1D. Estimated spectral power vs. angular frequency and $\Delta\phi_{mid}$. $\omega_1 = -\omega_2 = 2\pi/20$. N = 21. M = 19. $\Delta\phi_{mid}$ stepped from $-\pi$ to $\pi$ in increments of $2\pi/9$ radians. $r = \sqrt{100}$. (Perspective projection.)

22



Figure 7. Case 1E. Estimated spectral power vs. angular frequency and $\Delta\phi_{mid}$. $\omega_1 = -\omega_2 = 2\pi/20$. $N = 21$. $M = 19$. $\Delta\phi_{mid}$ stepped from $-\pi$ to $\pi$ in increments of $2\pi/9$ radians. $r = \sqrt{1000}$. (Perspective projection.)



Figure 8. Case 1F. Estimated spectral power vs. angular frequency and $\Delta\phi_{mid}$. $\omega_1 = -\omega_2 = 2\pi/20$. $N = 21$. $M = 19$. $\Delta\phi_{mid}$ stepped from $-\pi$ to $\pi$ in increments of $2\pi/9$ radians. $r = \infty$. (Perspective projection.)

powers of the signal poles were well represented by the real parts of the residues calculated at the estimated locations of the signal poles (even when the spectra showed gross variability in level, as in Case 1D (Figure 5)). Further, the residues corresponding to such apparently spurious spikes as are located slightly to the right of the signal poles in Figures 3 to 8 were negligible (always less than $10^{-6}$ of the signal power).

The absence of line-splitting is fully consistent with the theory of Section 4.2 as discussed in Section 4.3, since, for these data, (58) is satisfied in all instances: i.e., $G(N-1,\Delta\omega) = 0$ because $\sin[20x(2\pi/20)] \equiv 0$. Therefore at the stage M=2 of the Burg algorithm $\beta(2,2)$ was estimated according to (60) as $-1$, and the error output signals being processed at stages of the algorithm beyond M=2 were essentially white noise of low power. It appears that proceeding beyond the stage M=2 did not corrupt the estimated locations of the signal poles, at least when sufficient dynamic range (13 significant figures; floating-point arithmetic) is maintained in the processor.

Further examination of the signal powers estimated by the real part of the residues of the estimated signal poles revealed that, while the ratio $r^2$ of the signal powers was accurately maintained for all cases examined, the total signal power showed the modulation by the factor $\cos\Delta\phi_{mid}$, and that the depth of modulation was inversely proportional to $(r^2+r^{-2})$, as predicted by (53). These observations provide further confirmation of the validity of the theoretical results of Section 4.2.

## 5.2 CASE 2

The signal data for Case 2 consisted of 6 samples of two complex sinusoids with angular frequencies $\omega_{1,2} = \pm 2\pi/4$, so that $\Delta\omega=\omega_1$. $\Delta\phi_{mid}$ was varied from $-5\pi/2$ to $-\pi/2$ inclusive in 91 steps of $2\pi/90$ radians (4°). All spectra were estimated using (14) and a length 6 (M=5) PEF. Thus Case 2A (r=1) corresponds to Case 3 of Reference 8, where unit-amplitude real sine waves of frequency f = 5 Hz were each sampled six times at intervals $\Delta t = 0.05$ s as the initial phase $\phi_s$ was stepped between 0 and 180° in increments of 2°.

For this case $(N-1)\Delta\omega = 5x\ 2\pi/4 = 5\pi/2$ so that the data record contained an odd number of quarter cycles and $G(N-1,\Delta\omega) = 0.2 \neq 0$. Therefore, in light of (56) and (60) it would be expected that the Burg PEF would be biased and display dependence on $\cos\Delta\phi_{mid}$.

Substitution of N=6 and $\Delta\omega=\pi/2$ into (53) shows that $\Pi_2(0)$ is an unbiased estimate of the input signal plus noise power, so that fluctuations in the estimated signal powers made by the residue method are not expected. For this case (56) reduces to

$$<\beta_2(1,1)> = \left\{ \frac{j\rho(r) + 0.4\ \cos\Delta\phi_{mid}/(r^2+r^{-2})}{1 + 10^{-7.7}\ [1 + B_2(1,6)]} \right\} \tag{64}$$

and (60) reduces to

$$\beta_2(2,2) = -\left\{1 - 0.04\ \cos^2\Delta\phi_{mid}\right\} \Big/ \left\{1 + 0.04\ \cos^2\Delta\phi_{mid}\right\} \tag{65}$$

Consideration of (64) and (65) shows that here the Burg PEF should have greatest bias for r=1, when $(r^2+r^{-2})$ has its minimum value of 2, and that the bias should vanish for r=∞, when $\rho(r)=1$ and $\left|<\beta_2(1,1)>\right| \approx 1-4\times10^{-8}$. For the case r = ∞, (60) and hence (65) are not valid.

Examination of Figures 9 to 14 supports all these conjectures. These figures show orthographic projections of the 91 spectra, with ω ranging from −π to +π across the page, and $\Delta\phi_{mid}$ increasing "into" the page. The labelled vertical bar to the left of the spectra indicates a variation of 20 dB in power spectral density. It is clear that there is no line-splitting for $\Delta\phi_{mid}$ = −5π/2, −3π/2 and −π/2, and that the splitting shows a quasi-cosinusoidal dependence on $\Delta\phi_{mid}$ as suggested by the form of (64). The splitting became less severe as r→∞, again as might be inferred from (64), until for Case 2E the weaker signal pole was correctly estimated as a single pole. Examination of the zeroes of the PEFs and the residue powers showed measurable splitting of the stronger signal poles even for this case. Case 2F of course showed no line splitting, since there was then only one signal pole.

The "banding" effect visible most clearly in Figure 9 (Case 2A) and to a decreasing extent in subsequent figures can be explained on the basis that when $\cos\Delta\phi_{mid} = 0$, $\left|\beta_2(2,2)\right| \approx 1$ so that the output error power was greatly reduced in those cases. This caused a shift in the level of the spectrum, as can be seen from the dependence through (8b) of the numerator of (14) on this quantity. This also explains the obvious drop in spectral level in Figure 14, where $\left|\beta_2(1,1)\right| \approx 1$ for all values of $\Delta\phi_{mid}$.
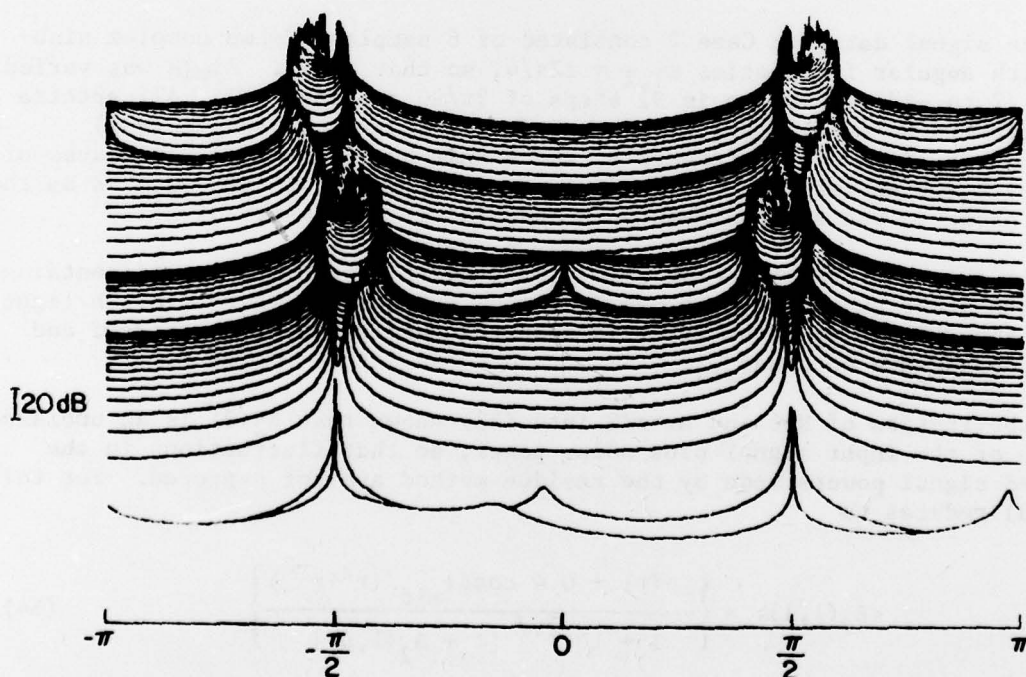


Figure 9. Case 2A. Estimated spectral power vs. angular frequency and $\Delta\phi_{mid}$. $\omega_1 = -\omega_2 = \pi/2$. N = 6. M = 5. $\Delta\phi_{mid}$ stepped from −5π/2 to −π/2 in increments of 2π/90 radians. r = 1. (Orthographic projection.)
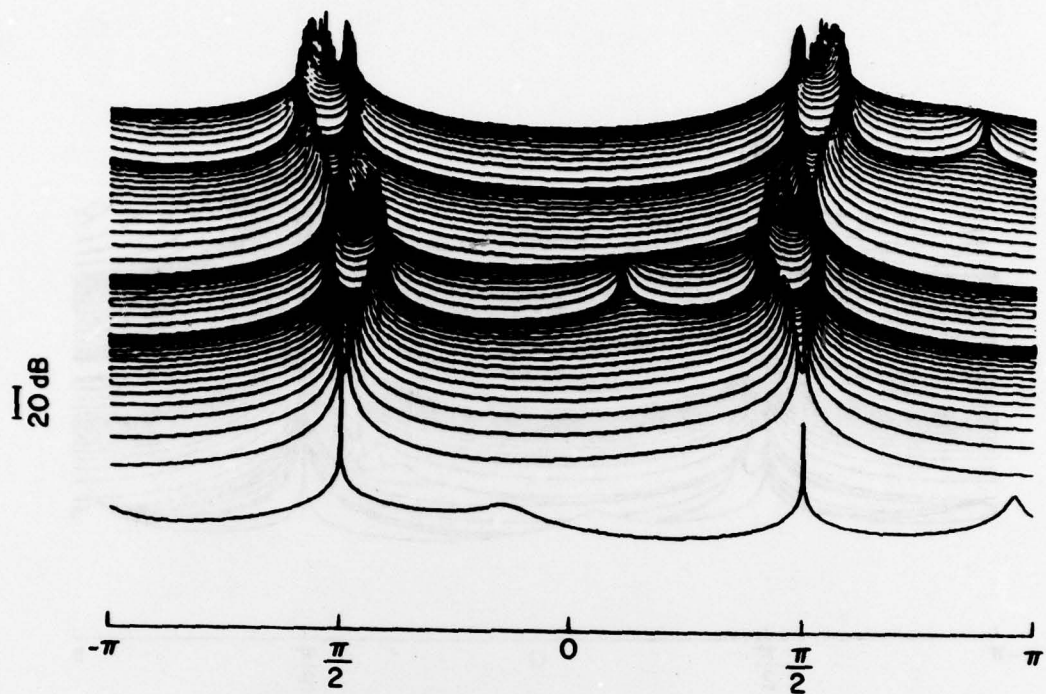
Figure 10. Case 2B. Estimated spectral power vs. angular frequency and $\Delta\phi_{mid}$. $\omega_1 = -\omega_2 = \pi/2$. N = 6. M = 5. $\Delta\phi_{mid}$ stepped from $-5\pi/2$ to $-\pi/2$ in increments of $2\pi/90$ radians. $r = \sqrt{2}$. (Orthographic projection.)



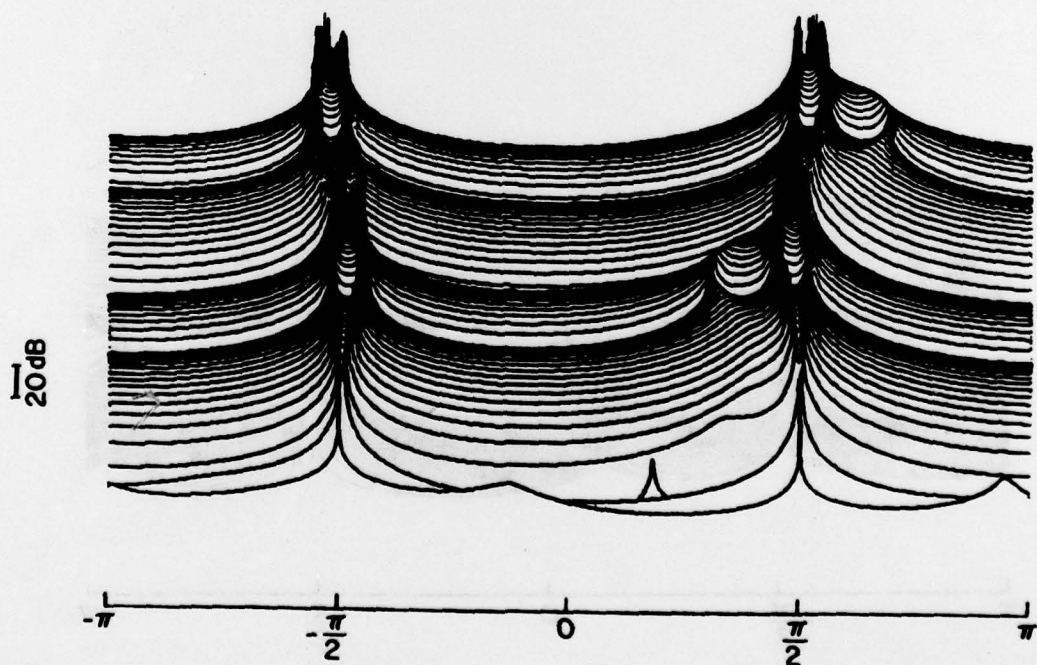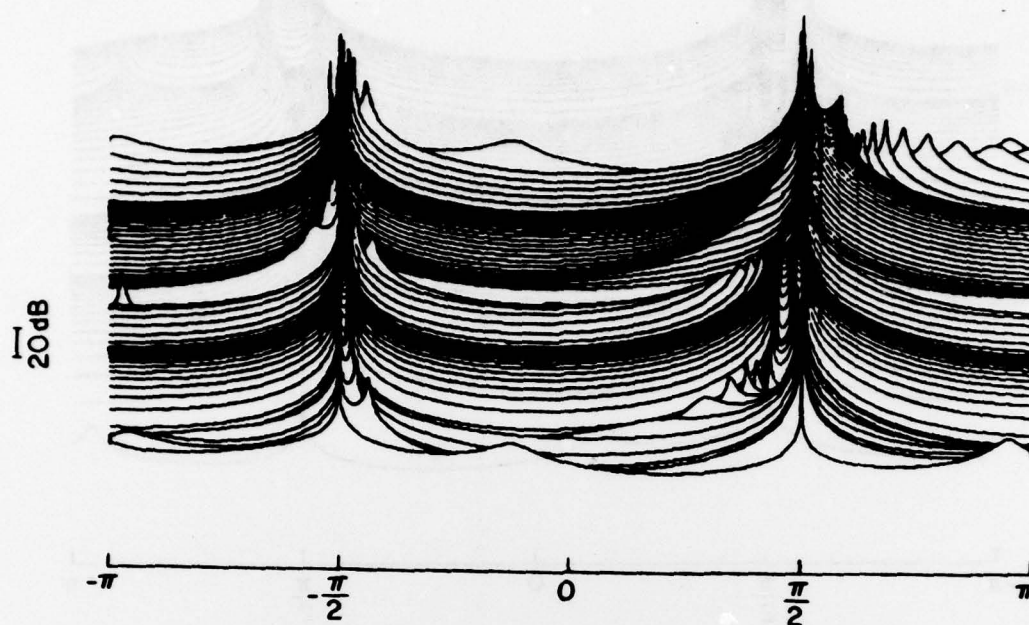Figure 11. Case 2C. Estimated spectral power vs. angular frequency and $\Delta\phi_{mid}$. $\omega_1 = -\omega_2 = \pi/2$. N = 6. M = 5. $\Delta\phi_{mid}$ stepped from $-5\pi/2$ to $-\pi/2$ in increments of $2\pi/90$ radians. $r = \sqrt{10}$. (Orthographic projection.)

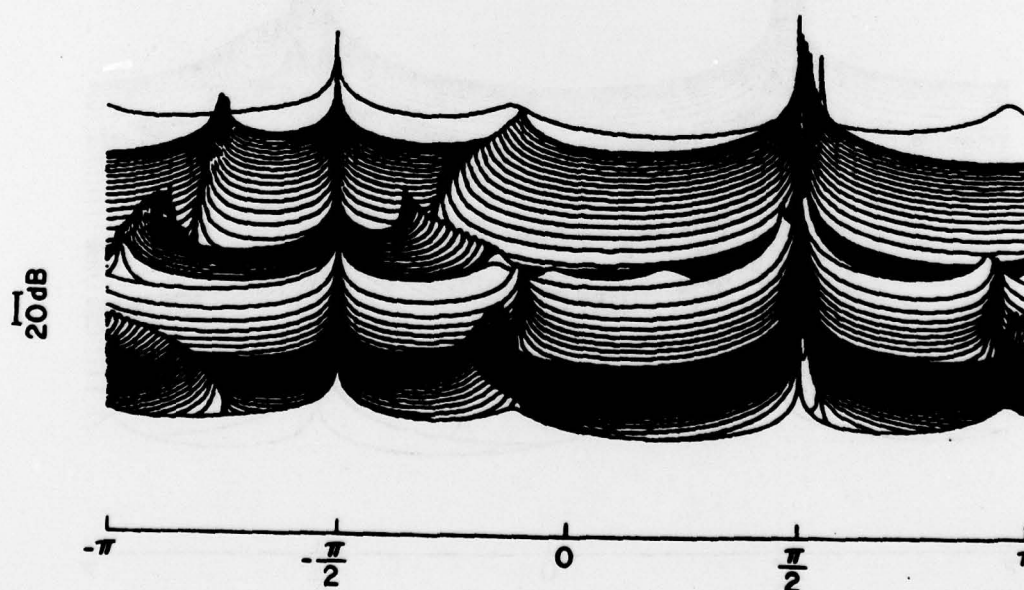Figure 12. Case 2D. Estimated spectral power vs. angular frequency and $\Delta\phi_{mid}$. $\omega_1 = -\omega_2 = \pi/2$. N = 6. M = 5. $\Delta\phi_{mid}$ stepped from $-5\pi/2$ to $-\pi/2$ in increments of $2\pi/90$ radians. $r = \sqrt{100}$. (Orthographic projection.)



Figure 13. Case 2E. Estimated spectral power vs. angular frequency and $\Delta\phi_{mid}$. $\omega_1 = -\omega_2 = \pi/2$. N = 6. M = 5. $\Delta\phi_{mid}$ stepped from $-5\pi/2$ to $-\pi/2$ in increments of $2\pi/90$ radians. $r = \sqrt{1000}$. (Orthographic projection).
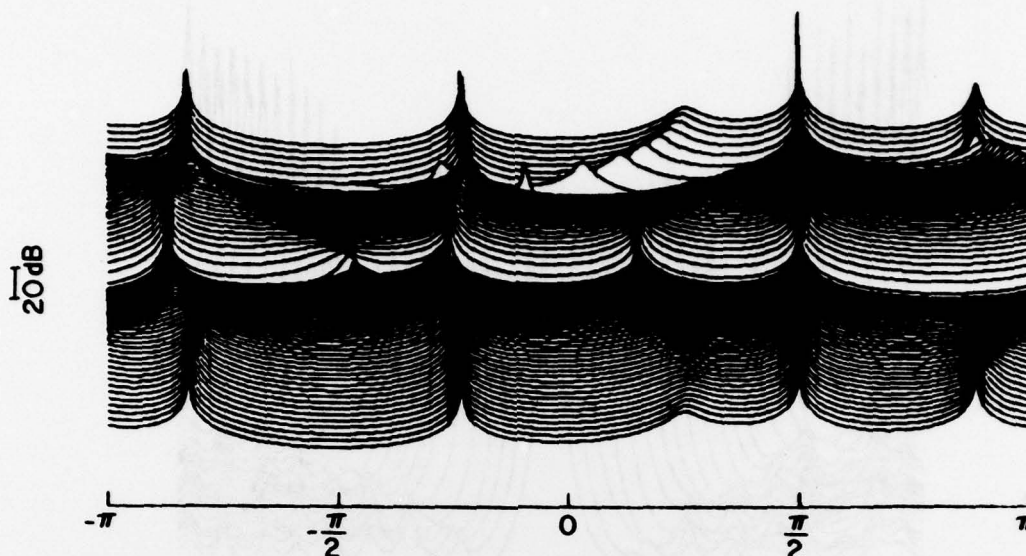
Figure 14. Case 2F. Estimated spectral power vs. angular frequency and $\Delta\phi_{mid}$. $\omega_1 = -\omega_2 = \pi/2$. $N = 6$. $M = 5$. $\Delta\phi_{mid}$ stepped from $-5\pi/2$ to $-\pi/2$ in increments of $2\pi/90$ radians. $r = \infty$. (Orthographic projection.)

Examination of the residue powers showed that, when line-splitting occurred, a significant portion of the signal power was accounted for by each pole of a split pair; in fact for Case 2A and $|\cos\Delta\phi_{mid}| \approx 1$, 70% of the signal powers appeared at the more severely deviated poles, and only 30% at less severely deviated poles. That the greater portion of the signal power was associated with the more deviated pole appeared for these data to be true in general. The present theory makes no prediction as to why this should be the case, although in principle the theory for the infinite SNR model could be extended to do so.

## 5.3 CASE 3

The signal data for Case 3 consisted of 25 sets of 101 samples of two complex sinusoids with $\Delta\phi_{mid} = 2\pi$ in all cases. Again $\omega_0 = 0$ was chosen, and $\Delta\omega$ was stepped from $2\pi \times 0.0125$ to $2\pi \times 0.4925$ inclusive in increments of $2\pi \times 0.02$. Thus Case 3A parallels Case 4 of Reference 8, where 101 samples were taken at intervals $\Delta t = 0.01$ s of real unit-amplitude sine waves with $\phi_s = \pi/4$ and $f_s$ stepped from 1.25 Hz to 49.25 Hz inclusive in steps of 2 Hz. In all cases the spectra were estimated using (14) and a length 25 (M=24) Burg PEF.

Figures 15 to 20 (Cases 3A to 3F) show the spectral estimates obtained from the data. These figures are again orthographic projections with $\Delta\omega$ increasing "into" the page. Any comments on the detailed structure of the line-splitting shown would necessarily be speculative, but some general observations can be made.
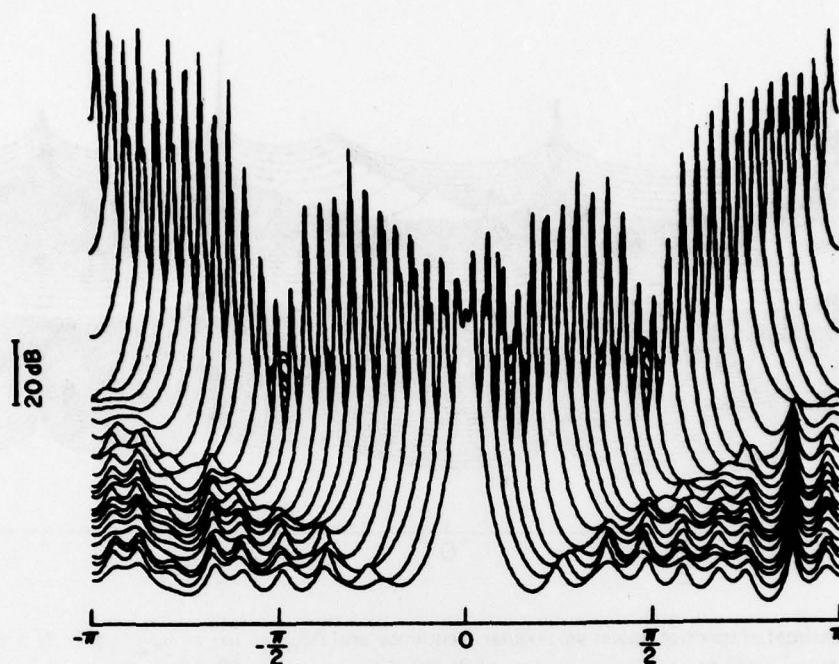
Figure 15. Case 3A. Estimate spectral power vs. angular frequency. $\Delta\phi_{mid} = 2\pi$. N = 101. M = 24. $\omega_1 = -\omega_2$ stepped from $2\pi \times 0.0125$ to $2\pi \times 0.4925$ in increments of $2\pi \times 0.02$. r = 1. (Orthographic projection.)
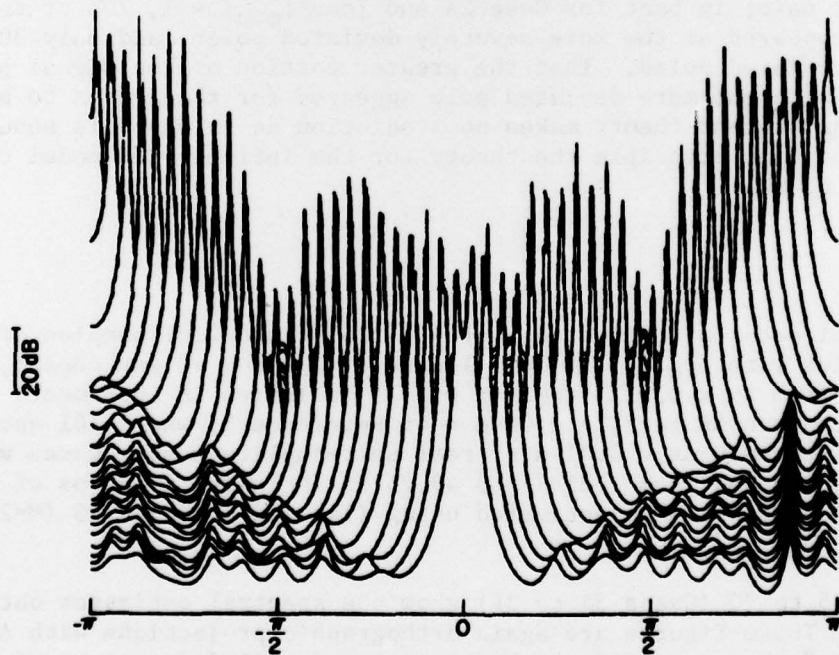


Figure 16. Case 3B. Estimate spectral power vs. angular frequency. $\Delta\phi_{mid} = 2\pi$. N = 101. M = 24. $\omega_1 = -\omega_2$ stepped from $2\pi \times 0.0125$ to $2\pi \times 0.4925$ in increments of $2\pi$ 0.02. $r = \sqrt{2}$. (Orthographic projection)

Figure 17. Case 3C. Estimate spectral power vs. angular frequency. $\Delta\phi_{mid} = 2\pi$. N = 101. M = 24. $\omega_1 = -\omega_2$ stepped from $2\pi$ x 0.0125 to $2\pi$ x 0.4925 in increments of $2\pi$ x 0.02. r = $\sqrt{10}$. (Orthographic projection.)



Figure 18. Case 3D. Estimate spectral power vs. angular frequency. $\Delta\phi_{mid} = 2\pi$. N = 101. M = 24. $\omega_1 = -\omega_2$ stepped from $2\pi$ x 0.0125 to $2\pi$ x 0.4925 in increments of $2\pi$ x 0.02. r = $\sqrt{100}$. (Orthographic projection.)

Figure 19. Case 3E. Estimate spectral power vs. angular frequency. $\Delta\phi_{mid} = 2\pi$. N = 101. M = 24. $\omega_1$ $-\omega_2$ stepped from $2\pi \times 0.0125$ to $2\pi \times 0.4925$ in increments of $2\pi \times 0.02$. $r = \sqrt{1000}$. (Orthographic projection.)
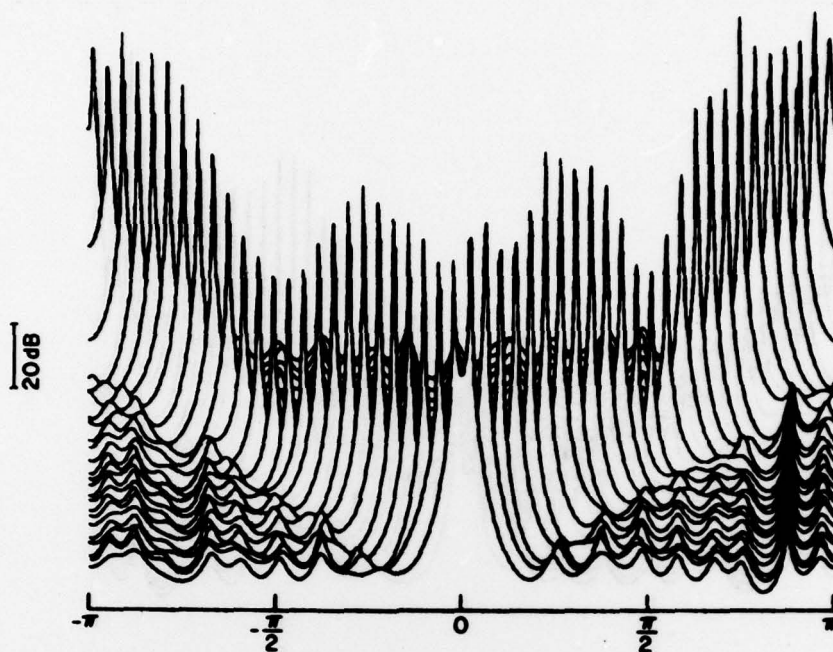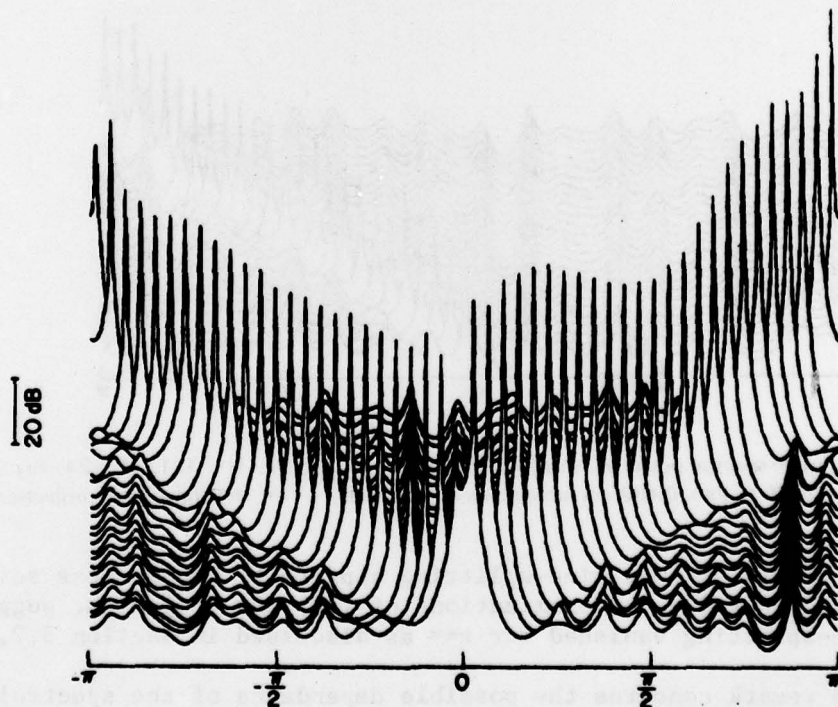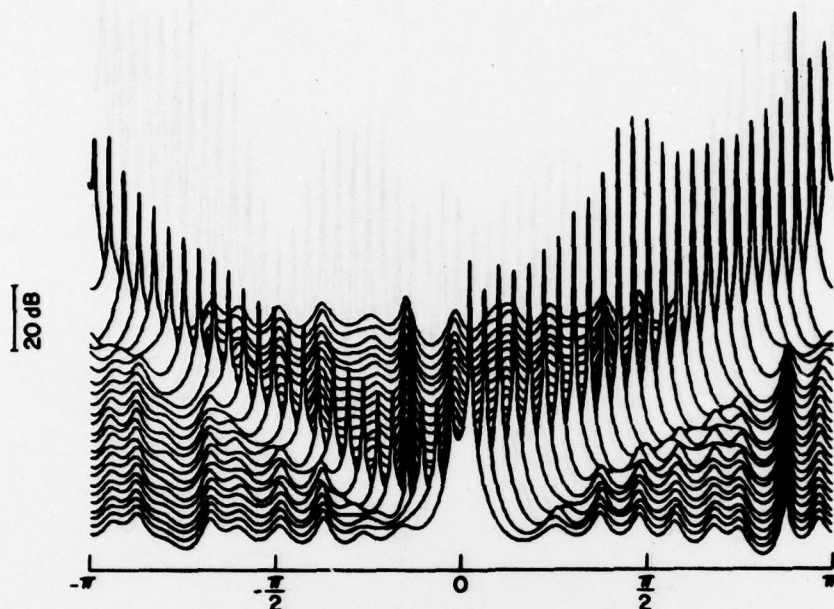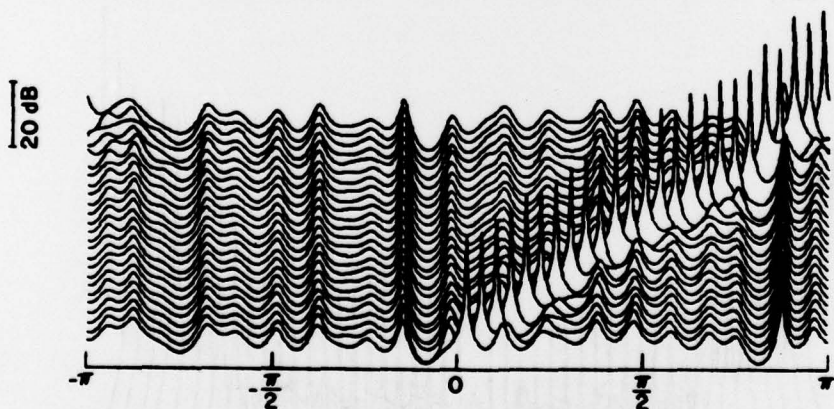


Figure 20. Case 3F. Estimate spectral power vs. angular frequency. $\Delta\phi_{mid} = 2\pi$. N 101. M 24. $\omega_1$ $-\omega_2$ stepped from $2\pi \times 0.0125$ to $2\pi \times 0.4925$ in increments of $2\pi \times 0.02$. r ∞. (Orthographic projection.)

The first remark is that line-splitting appears to become less severe as r was increased in value, as examinations of (56) and (60) might suggest, and in fact line-splitting vanished for r=∞ as discussed in Section 5.2.

The second remark concerns the possible dependence of the spectral level on the values of $G(N-1,\Delta\omega)$ and $G(N-2,\Delta\omega)$. These values are given for the plotted spectra in Table 2. It is interesting to note that the minimum spectral level occurred at the minimum values for $|G(N-1,\Delta\omega)|$, $|G(N-2,\Delta\omega)|$

and $|\cos\Delta\omega|$, and that higher spectral levels were observed when $G(N-2,\Delta\omega)$ < 0, or $\Delta\omega > 2\pi \times 0.25$. Examination of (60) shows that as $\Delta\omega$ exceeds the value $\pi/2$ certain terms change sign in such a manner as to decrease the magnitude of $\beta_2(2,2)$ and thus perhaps to increase the magnitude of the numerator of (14) through the relation (8b).

Finally, for Case 3F it is again observed that the spectral level drops as $r\to\infty$ and the bias term in (56) vanishes, similar to Case 2F. For Case 3F only, the estimated poles accurately reflected the true signal pole locations, were unsplit and had correct residue powers. For all other cases, examination of the locations of the poles of the Burg spectral estimate showed the existence of multiple poles with significant residue power in the vicinity of the true locations of the two signal poles.

### TABLE 2

*Values of $(\Delta\omega/2\pi) \times 100$, $G(N-1,\Delta\omega)$ and $G(N-2,\Delta\omega)$ for Data from Case 3*

| $(\Delta\omega/2\pi) \times 100$ | $G(N-1,\Delta\omega)$ | $G(N-2,\Delta\pi)$ | $\cos\Delta\omega$ |
|---|---|---|---|
| 1.25 | 0.1275 | 0.1823 | 0.9969 |
| 3.25 | 0.0493 | 0.0488 | 0.9792 |
| 5.25 | 0.0309 | 0.0295 | 0.9461 |
| 7.25 | 0.0227 | 0.0206 | 0.8980 |
| 9.25 | 0.0182 | 0.0125 | 0.8358 |
| 11.25 | 0.0154 | 0.0118 | 0.7604 |
| 13.25 | 0.0135 | 0.0092 | 0.6730 |
| 15.25 | 0.0122 | 0.0071 | 0.5750 |
| 17.25 | 0.0113 | 0.0053 | 0.4679 |
| 19.25 | 0.0107 | 0.0038 | 0.3535 |
| 21.25 | 0.0103 | 0.0024 | 0.2334 |
| 23.25 | 0.0101 | 0.0011 | 0.1097 |
| 25.25 | 0.0100 | -0.0002 | -0.0157 |
| 27.25 | 0.0101 | -0.0014 | -0.1409 |
| 29.25 | 0.0104 | -0.0028 | -0.2639 |
| 31.25 | 0.0108 | -0.0042 | -0.3827 |
| 33.25 | 0.0115 | -0 0058 | -0.4955 |
| 35.25 | 0.0125 | -0.0076 | -0.6004 |
| 37.25 | 0.0135 | -0.0098 | -0.6959 |
| 39.25 | 0.0160 | -0.0126 | -0.7804 |
| 41.25 | 0.0191 | -0.0165 | -0.8526 |
| 43.25 | 0.0243 | -0.0224 | -0.9114 |
| 45.25 | 0.0340 | -0.0328 | -0.9558 |
| 47.25 | 0.0582 | -0.0579 | -0.9551 |
| 49.25 | 0.2123 | -0.2142 | -0.9889 |

## 6. SUMMARY AND CONCLUSIONS

The theoretical properties of autoregressive spectral analysis schemes have been analyzed when the signal under investigation is known to be comprised of one or two complex sinusoids in additive white noise. This latter case includes as a special case data comprising a single real sine wave in additive white noise. It has been shown that when the autocorrelation of the signal is known, the frequency of a single complex sinusoid can always be extracted, independent of the signal-to-noise ratio (SNR), provided enough samples of the autocorrelation are available. It was also shown that the Burg algorithm correctly extracts the frequency of a single sinusoid in additive white noise from the complex amplitude time-series data, provided the SNR is sufficiently high.

The situation when two complex sinusoids are present is much more complicated. It was found to be fairly difficult to derive general equations describing the spectrum for the known autocorrelation (KA) case, even for a two-pole autoregressive model. Nevertheless these equations served as a useful touchstone for the extremely complicated Burg equations for the analysis of time-series amplitude data. Detailed theoretical analysis showed that, unlike the KA case, the Burg spectral estimate is expected to be sensitive both to the number of cycles of the difference frequency between the two components contained in the finite-length data record, and in particular to the relative phase difference between the two complex sinusoidal components at the middle of the data record. Finally, simulation results were shown to be fully compatible with the conjectured basis of line-splitting presented here.

## 7. ACKNOWLEDGEMENT

## 8. REFERENCES

1.   Burg, J.P., *Maximum Entropy Spectral Analysis*, presented at the 37th Meeting of the Society of Exploration Geophysicists, Oklahoma City, 31 October 1967.

2.   Burg, J.P., *A New Analysis Technique for Time Series Data*, presented at the NATO Advanced Study Institute on Signal Processing with Emphasis on Underwater Acoustics, Enschede, Netherlands, 1968.

3.   Burg, J.P., *Maximum Entropy Spectral Analysis*, Ph.D. Thesis Stanford University, Stanford, California, May 1975.

4.   Ulyrch, T.J. and R.W. Clayton, *Time Series Modelling and Maximum Entropy*, Phys. Earth Planet. Inter., 12, 1976, pp. 188-200.

5.   Frost, O.L., *Power Spectrum Estimation*, in Aspects of Signal Processing, Part 1, D. Reidel Publishing Company, Dordrecht-Holland, 1977, pp. 125-162.

6.   Marple, L.A., *Conventional Fourier, Autoregressive, and Special ARMA Methods of Spectrum Analysis*, Engineer's Degree Thesis, Stanford University, Stanford, California, December 1976.

7.   Chen, W.Y. and G.R. Stegen, *Experiments with Maximum Entropy Power Spectra of Sinusoids*, J. Geophys. Res., 79, No. 20, 10 July 1974, pp. 3019-3022.

8.   Fougere, P.F., E.J. Zawalick and H.R. Radoski, *Spontaneous Line Splitting in Maximum Entropy Power Spectrum Analysis*, Phys. Earth Planet. Inter. 12, 1976, pp. 201-207.

9.   Fougere, P.F., *A Solution to the Problem of Spontaneous Line Splitting in Maximum Entropy Power Spectrum Analysis*, J. Geophys. Res., 82, No. 7, 1 March 1977, pp. 1051-1054.

10.  Makhoul, J., *Linear Prediction: A Tutorial Review*, Proc. IEEE, 63, No. 4, April 1975, pp. 561-580.

11.  Makhoul, J., *Lattice Methods in Spectral Estimation*, Proceedings of the RADC Spectrum Estimation Workshop, 24, 25 and 26 May 1978, pp. 159-173, AD-A054650.

12.  Smylie, D.E., G.K.C. Clarke and T.J. Ulrych, *Analysis of Irregularities in the Earth's Rotation*, Methods in Computational Physics, 13, Academic Press, New York, 1973, pp. 391-430.

13.  Andersen, N., *On the Calculation of Filter Coefficients for Maximum Entropy Spectral Analysis*, Geophysics 39, No. 1, February 1974, pp. 69-72.

14.  Herring, R.W., *A Review of Maximum Entropy Spectral Analysis*, CRC Technical Note 685, June 1977.

15.  Johnsen, S.J. and N. Andersen, *On Power Estimation in Maximum Entropy Spectral Analysis*, Geophysics 43, No. 4, June 1978, pp. 681-690.

# A P P E N D I X   A

## A Bias Term

The bias term $B_2(1,N)$ found in the expression for $<\beta_2(1,1)>$ is:

$$B_2(1,N) = (N-1)^{-1}\left\{1 + [(N-2)/(N-1)] \times\right.$$

$$[\cos\Delta\omega + j\rho(r)\sin\Delta\omega + \cos\Delta\phi_{mid}\cos\Delta\omega G(N-2,\Delta\omega)/(r^2+r^{-2})] \qquad (A1)$$

$$\left. \Big/ [\cos\Delta\omega + j\rho(r)\sin\Delta\omega + 2\cos\Delta\phi_{mid}\cos\Delta\omega G(N-1,\Delta\omega)/(r^2+r^{-2})]\right\}$$